Metal-induced gap states

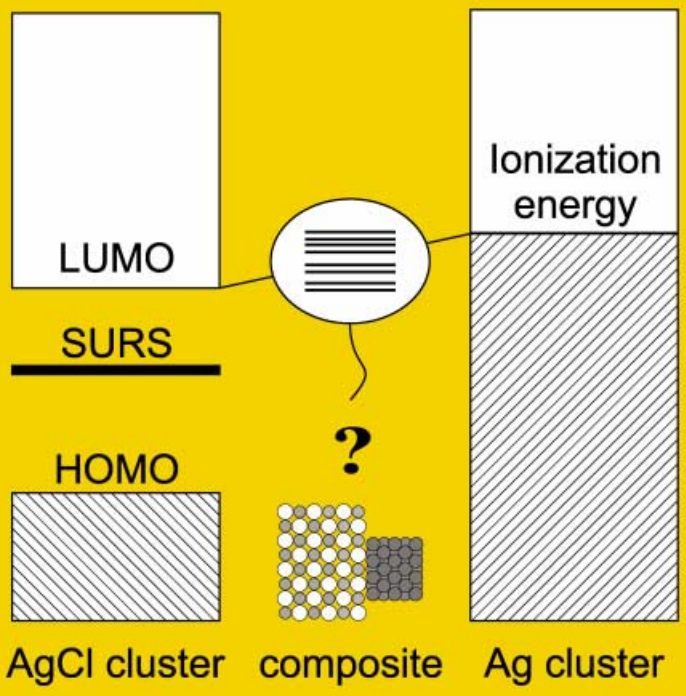

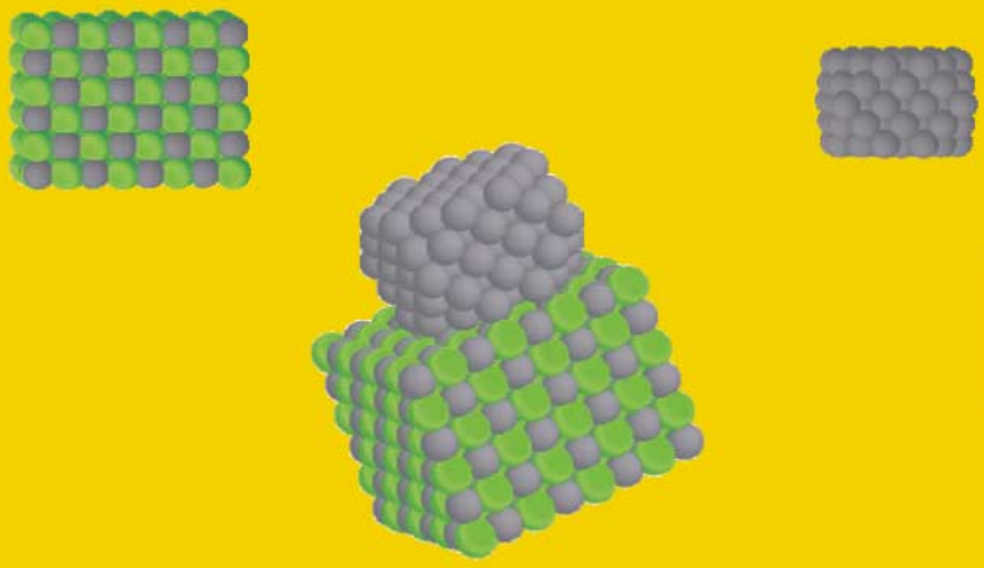

For more information see the following pages.

What happens at the interface, in terms of electronic states and charge distribution, when a semiconductor and a metal cluster are brought into contact?

  0947-6539/02/0808-1785 $ 20.00+.50/0

Electronic Properties of the Silver–Silver Chloride Cluster Interface

Stephan Glaus,[a] Gion Calzaferri,*[a] and Roald Hoffmann*[b]

Abstract: The objective of this study was to gain insight into the electronic structure of silver–silver chloride cluster composites and especially into the metal–semiconductor interface. For this purpose a theoretical study of $(AgCl)_n$ ($n = 4$, 32, 108, 192, and 256), of Ag_m ($m = 1-9$, 30, 115, 276, and 409), and of the cluster composites $Ag_{115}-(AgCl)_{192}$ and $Ag_{409}-(AgCl)_{192}$ has been carried out. Density of levels (DOL), local density of levels (*l*-DOL), and projection of surface states, as well as projection of properties of individual atoms or groups of atoms obtained in molecular orbital calculations, are shown to be powerful tools for gaining deep insight into the properties of these large systems. The $Ag_{115}-(AgCl)_{192}$ aggregate, consisting of a cubic Ag_{115} cluster without corner atoms on top of a cubic $(AgCl)_{192}$ cluster, was found to be remarkably stable with a cluster-to-cluster distance of about 280 pm, and a geometry in which the number of bonding interactions between the silver atoms of Ag_{115} and the chloride ions of $(AgCl)_{192}$ is at its maximum. A sharp jump in charge distribution occurs at the $Ag_{115}-(AgCl)_{192}$ composite interface. The first AgCl slab picks up negative charge from the two adjacent silver slabs, so that in total the silver cluster is positively charged. In addition, the core of the silver cluster is positively charged with respect to its outermost layer. The main reason for the charge transfer from the silver cluster to the silver chloride is the newly formed MIGS (metal induced gap states) in the energy-gap range of the silver chloride and the MIdS (metal induced d states) in the d-orbital region. Their wave functions mix with orbitals of the silver cluster and with both the orbitals of the silver and the chloride ions of the silver chloride. The MIGS and the MIdS are of a quite localized nature. In them, nearest neighbor interactions dominate, with the exception of close-lying silver chloride surface states—which mix in to a large extent. We conclude that especially the MIGS not only influence the photochemical properties of silver chloride, but that their existence might be probed by appropriate spectroscopic measurements.

Keywords: cluster compounds · interfaces · nanostructures · silver · silver chloride

Introduction

Metal–semiconductor contacts have been the subject of various investigations for over 100 years. Their behavior led to the discovery of Schottky and Ohmic contacts and to the concept of band bending, illustrated in Figure 1.[1–4] In the simple Schottky theory, the contact type depends on the relative energy position of the semiconductor band gap with respect to the metal work function. The bending of the conduction and valence band is due to a change in the electrical potential, $-e\phi$, which is caused by electron transfer at the interface region.

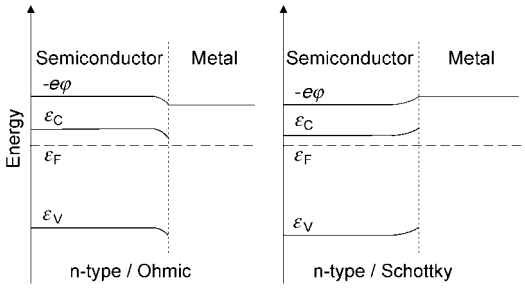

Figure 1. Band representation of an n-type semiconductor in contact with a metal, showing how metals with low work functions lead to Ohmic contacts and metals with high work functions form Schottky contacts. $-e\phi$, ε_C, ε_F, and ε_V represent the electrical potential, the conduction band energy, the Fermi level, and the valence band energy, respectively.[3]

Microscopic and atomistic cluster aspects are missing in Figure 1. What does happen at the interface, in terms of electronic states and charge distribution, when two clusters are brought into contact, as shown schematically in Figure 2?

Large single-crystal or dense AgCl materials are only slightly light sensitive. Pronounced light sensitivity is observed

[a] Prof. G. Calzaferri, Dipl.-Chem. S. Glaus
Department of Chemistry and Biochemistry
University of Bern, Freiestrasse 3, 3012 Bern (Switzerland)
Fax: (+41) 31-6313994
E-mail: gion.calzaferri@iac.unibe.ch

[b] Prof. R. Hoffmann
Department of Chemistry and Chemical Biology
Cornell University, Baker Laboratory, Ithaca, NY, 14853-1301 (USA)
Fax: (+1) 607-255-5707
E-mail: rh34@cornell.edu

  0947-6539/02/0808-1786 $ 20.00+.50/0

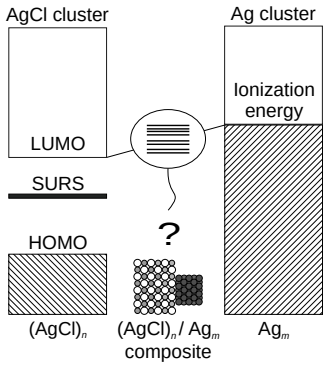

Figure 2. Energy level diagram of a Ag_m and a $(AgCl)_n$ cluster. The figure illustrates schematically the new states built up at the interface upon interaction of the clusters. These interface levels (Metal induced gap states) influence the electronic properties of the cluster composite and are the main point of interest in our study.

for AgCl materials with large surfaces see for example ref. [5]. Defects in crystals may give rise to states similar to those created by surface atoms. The interaction of metal particles on semiconductor surfaces, which is a complex problem due to the variety of processes involved, has been experimentally investigated on many surfaces.[6–9] However, a theoretical study of a metal–semiconductor cluster interface on a system of relevant size remains challenging. One reason for this is the rapidly increasing number of atoms in such clusters. We have recently shown that molecular-orbital calculations are well suited for studying the electronic structure of AgCl crystals, of AgCl clusters, and of hydrated silver ions, as well as for advancing our understanding of silver ions in zeolites.[10, 11] This has encouraged us to undertake theoretical investigations on the $(AgCl)_n$, Ag_m, and the $Ag_m-(AgCl)_n$ composites shown in Figure 3.

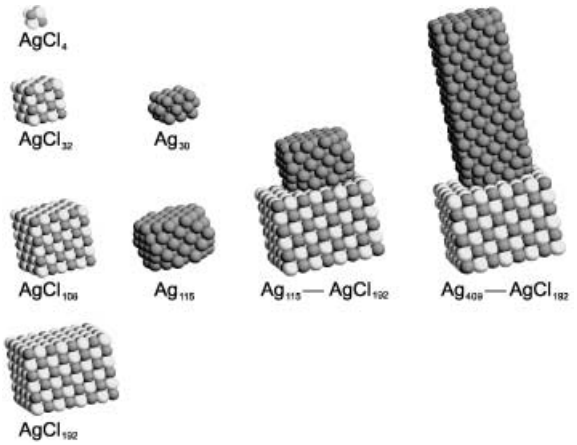

Figure 3. Clusters and composites studied in this and former work.[10] The silver atoms and the silver ions are shown in dark gray, while the chloride ions are light gray.

While the calculation of large systems consisting of several hundred up to a few thousand atoms depends mainly on the computer power available, the extraction of relevant qualitative information from the vast array of generated numbers does not become any easier if one has great resources. There is too much information in the individual energy levels. Even the frontier-orbital region is not easy to survey. However, tools and concepts such as LCFMO,[12] the density of levels (DOL), the local-DOL (*l*-DOL),[13, 14] and more recently the density of transitions[11] have been shown to be very powerful. The technique of projection of surface states[15] (what a chemist would call contributions of surface states), as discussed in ref. [12], has been recently generalized.[10] A further tool which we will show to be useful for analyzing large clusters is the projections of properties of individual atoms or groups of atoms. The main question addressed in this study is: How can $Ag_m-(AgCl)_n$ composites be described and what are their properties? This raises some additional questions such as: How large must a system be for inner atoms to be regarded as bulk atoms? Can we distinguish localized energy levels at the interface? What are the properties of atoms located at the metal–semiconductor interface? What is the charge distribution at the interface? Do surface states (SURS) influence the interface properties? We show that the methods applied in this study lead to exciting new insights, which, in turn, we hope will stimulate future experimental work.

Computational Methods

Molecular orbital (MO) calculations: Extended Hückel molecular orbital (EHMO)[16] and tight binding (EHTB)[17] calculations in their ASED (atomic superposition and electron delocalization) form[18, 19] were performed by using the ICON-EdiT[20] and BICON-CEDiT[21] program packages, respectively. The off-diagonal elements were calculated by using the modified distance-dependent weighted Wolfsberg–Helmholz formula explained in ref. [22] with $\kappa = 0.8$, $\delta = 0.35\,\text{Å}^{-1}$. The Coulomb parameters H_{ii} and H_{ij} of the *i*th and *j*th atomic orbital have been determined by a revised self-consistent charge configuration (SCCC) procedure. Details are given in the appendix. The Slater parameters listed in Table 1 and SCCC parameters in Table 2 were used. Densities of states (DOS) were determined by using a set of 100 *k* points representing the face centered cubic lattice.[23]

Table 1. Slater exponents

Element	AO	ζ_1	ζ_2	c_1	c_2
Cl	3s	2.50			
	3p	1.73			
Ag^+	5s	1.85			
	5p	1.30			
	4d	3.91	1.54	0.824	0.329
Ag^0	5s	1.70			
	5p	1.30			
	4d	3.91	1.54	0.824	0.329

Density of levels (DOL): The calculated extended Hückel wave functions and respective energies were subsequently used to compute the density of levels (DOL).[13] We make use of the terms DOL and *l*-DOL. The DOL counts the number of discrete energy levels (molecular orbitals) in a given (small) energy range. In its limiting case for very large systems, it is identical to the density of states (DOS), familiar from solid state physics.[17] The half width of the Gaussian function used to fit the DOL was 0.05 eV. A local DOL (*l*-DOL) is the contribution to the DOL of an atom group or a single atom. The concept is related to the atomic orbital projections in the EHTB method. It provides useful information, for example allowing us to distinguish properties of surface atoms from those of bulk atoms. In this projection procedure, the electron occupation for the specified atom is

Table 2. Self Consistent Charge Configuration Parameters.

	Configuration	d_2 [eV]	d_1 [eV]	d_0 [eV]
Silver				
sVOIE	$4d^{10}5s^1$	0.5500	8.3900	7.5800
	$4d^9 5s^2$	0.3700	8.8800	8.8000
	$4d^9 5s^1 5p^1$	0.3100	9.7100	10.2300
pVOIE	$4d^{10}p^1$	0.7700	6.4600	3.8300
	$4d^9 p^2$	1.1800	6.8600	8.1200
	$4d^9 5s^1 5p^1$	1.1800	6.8600	4.7600
dVOIE	$4d^{10}$	−3.9000	25.6000	0.0000
	$4d^{10}5s^1$	0.4600	12.6600	12.7700
	$4d^{10}5p^1$	0.8100	11.6700	14.4900
Chlorine[a]				
sVOIE	$3s^2 3p^5$	1.6986	15.7089	25.2682
pVOIE	$3s^2 3p^5$	1.6726	13.1796	13.6880

[a] Ref. [24].

calculated by means of the Mulliken population analysis.[25] The occupation number thus obtained is multiplied by the total DOL. After normalization it can be compared with the total DOL or with another projected DOL.[11]

Annotation of the composites: Figure 4 shows the numbering of the layers used for the $Ag_{115}-(AgCl)_{192}$ composites. Layers 1 to 6 belong to the AgCl cluster, layers 7 to 11 to the Ag cluster. The two cuts I and II are used to distinguish surface properties from bulk properties, in a sequence of numerical experiments to be described below. They also apply to the $Ag_{409}-(AgCl)_{192}$ composite. We distinguish three situations: a) in which all atoms are taken into account (= total). b) in which all atoms except the outermost shell of the silver cluster are considered (= cut I) and c) in which only the core of the silver cluster is considered (= cut II). We also show the rotation coordinate used in the geometry optimization.

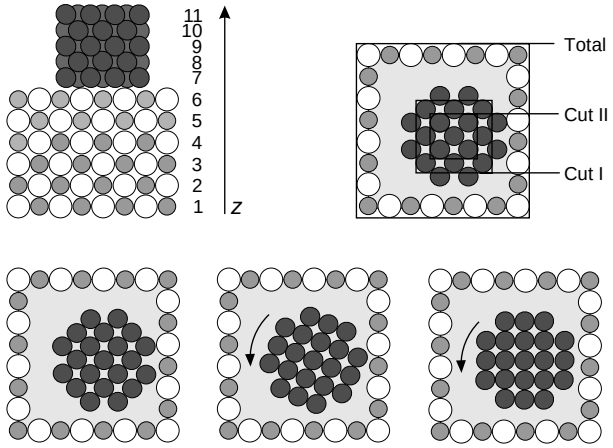

Figure 4. Numbering of the layers of the $Ag_{115}-(AgCl)_{192}$ composite and definition of the two cuts we are using. In addition, the rotation of the Ag_{115} cluster around its center on top of the $(AgCl)_{192}$ is shown.

Results and Discussion

The objective of this study is to gain insight into the electronic structures of the $Ag_m-(AgCl)_n$ cluster composites and especially into the metal–semiconductor interface. This goal can be achieved by performing calculations for the clusters shown in Figure 3. A detailed investigation of $(AgCl)_n$ clusters was published recently[10] and will only be reviewed briefly. We then report relevant data for silver clusters, before proceeding to the $Ag_m-(AgCl)_n$ composites.

$(AgCl)_n$ clusters: It is well established that the (100) surface of AgCl is by far the most stable.[26] Cubic $(AgCl)_n$ clusters have therefore been investigated in some detail. We found that the computational results obtained for the AgCl molecule, for an infinite AgCl crystal, but also for hydrated silver ions are in good agreement with experimental results.[10] Based on this, the AgCl bond length and the electronic structure of four different $(AgCl)_n$ clusters ($n=4$, 32, 108, and 256) were investigated. The calculated AgCl bond lengths show an increase of 0.13 Å from $(AgCl)_4$ to $(AgCl)_{32}$ but the changes become smaller for larger clusters, only 0.02 Å, for example, on going from $(AgCl)_{108}$ to $(AgCl)_{256}$. The same is true for the HOMO–LUMO gap. The energy of the HOMO changes little even from the AgCl molecule to $(AgCl)_4$. This orbital consists of Cl-3p lone pairs while the LUMO is of a Ag-5s type. In the larger clusters, the LUMO is mainly localized at the corner atoms and can therefore be identified as a surface state (SURS). These SURS reduce the undisturbed crystal band gap by about 1 eV.[10]

Ag_m clusters:[27] Nanometer-scale clusters of materials have a demonstrated variety of applications ranging from catalysis,[28, 29] to optoelectronics,[30] photography,[31] surface-enhanced Raman spectroscopy[32] and electronic devices.[33] Silver clusters have recently also been used in studies on organic-based solar cells, in which they work as electron injectors.[34] We have been interested in the role of Ag clusters in photocatalytic water-splitting devices[5] that are based on silver chloride as photoanode.[35]

Silver clusters have been investigated experimentally and theoretically in many laboratories and for different purposes. We focus on properties relevant to the questions addressed in this paper, beginning with the first ionization potential, which has been measured for Ag_m, $m=1$, 2, …, 9.[36, 37] The experimental work functions for the different silver crystal surfaces are 4.14 eV, 4.22 eV, and 4.46 eV for (110), (100), and (111), respectively.[38] The comparison of the experimental values and our calculations in Table 3 and Figure 5 illustrate that the calculations reproduce the experimental trend nicely.

Table 3. Experimental, calculated ionization energies, symmetry and structure of Ag_n ($n=1, 2, 3, \ldots \infty$) clusters. Experimental values are taken from refs. [36–38].

$n(Ag_n)$	IP_{exp} [eV]	IP_{theor} [eV]	symmetry	structure
1	7.57	7.57	–	–
2	7.60	9.47	$D_{\infty h}$	line
3	6.20	5.95	D_{3h}	triangle
4	6.65	7.74	D_{2h}	rhombus
5	6.35	6.78	C_{2v}	planar triangular lattice
6	7.15	8.22	C_{5h}	pentagonal pyramid
7	6.40	7.29	D_{5h}	pentagonal bipyramid
8	7.10	7.98	O_h	cube
9	6.00	5.92	C_{4v}	capped square antiprism
30	–	5.32	D_{4h}	–
115	–	4.65	D_{4h}	–
276	–	4.39	D_{4h}	–
409	–	4.31	D_{4h}	–
∞	4.46 (111)	4.43	–	face centered cubic
∞	4.14 (110)		–	face centered cubic
∞	4.22 (100)		–	face centered cubic

0947-6539/02/0808-1788 $ 20.00+.50/0 *Chem. Eur. J.* **2002**, *8*, No. 8

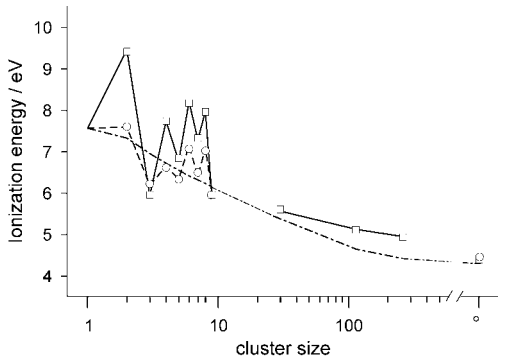

Figure 5. Ionization energies of Ag_n clusters ($n = 1, 2, \ldots, 276$) and the crystal calculated with the EHMO method (——□——) and the liquid drop model[42, 43] (–·–·–). Experimental values have also been added (----○----).

We are therefore confident that the theoretical values obtained for Ag_{30}, Ag_{115}, Ag_{276}, and Ag_{409} make sense. The structures we used rely on the theoretical results reported in refs. [39] and [40] for Ag_3 to Ag_9. Larger clusters are expected to be spherical in order to minimize their surface energy. We mimic them as cubic clusters without corner atoms. An exception is the Ag_{409} cluster, which was used for a special purpose, as will be seen. The results in Table 3 and Figure 5 show the well known odd–even oscillation, which is also present in alkali metal clusters.[41] This oscillation has its origin in the alternating single and double occupation of the HOMO. The EHMO calculations overestimate this oscillation because the electron–electron repulsion is only treated in average manner. This is also the reason why the ionization energy of Ag_2 is overestimated. The effect smoothes out, however, with increasing cluster size as the liquid-drop model starts to become a reasonably good approximation.[42, 43] Quantum chemical calculations of other groups for Ag_m ($m < 20$) lead to similar results. Theoretical and experimental absorption spectra of extended Ag crystals are discussed in ref. [44]. Electronic absorption spectra of small Ag_m clusters with $m =$ 2–21 are discussed in ref. [45].

The evolution of the electronic properties as a function of the cluster size and the influence of surface effects are best seen by analyzing the DOL and the *l*-DOL. The DOL of Ag_9 (1), Ag_{115} (2), Ag_{276} (3), and the DOS of Ag_∞(4) are shown in Figure 6. Also the projections (*l*-DOL) of Ag_{276} without the outermost surface layer (3a) and without the two outermost atomic shells (3b) are drawn. The DOS contributions of the s, p, and d orbitals have been projected for Ag_∞ and are shown on the right. The solid line marks the HOMO of (2), (3), and (4), which also corresponds to the first ionization energy. In the DOL of Ag_9 we can almost distinguish every single energy level, except in the d-orbital region at -13 to -11 eV, which is broadened due to numerous levels close to each other in energy. Ag_9 has an energy gap of about 1 eV. This gap has disappeared in Ag_{115}. Little changes upon increasing the size from Ag_{115} to Ag_{276}. These clusters already show the properties of large Ag particles. However, the cluster DOLs stemming from d levels differ significantly from the DOS of the bulk. The peak, marked with a circle in Figure 6, is missing in the cluster DOL for Ag_{276} and smaller clusters. The reason for this can be deduced when considering the *l*-DOLs (3a) and (3b). The peak shows up clearly in (3b), the part of the cluster with the outer shells removed. It follows that atoms lying at the surface have "buried" the indicated peak. The core of the cluster shows bulk properties. The difference between the DOL (3) and the *l*-DOLs (3a) and (3b) are due to dangling bonds (unsaturated coordination) at the surface. The SURS of small clusters up to Ag_9 have been discussed in the literature,[46–49] and the results reported agree well with our observations. Less information could be deduced from the DOL and DOS above -11 eV, composed primarily of s and some p states.

The bond lengths of the Ag_m clusters show a steep increase with size until about $m = 10$, at which point the atom-to-atom length observed in the bulk silver is reached. The calculated bulk distance is 3.1 Å, while the experimental value is 2.9 Å.[50, 51] We have used this latter value for all further calculations. Similar results were found by Bonačić-Koutecký et al.[39]

Ag_m–$(AgCl)_n$ composites: We have shown that important properties of Ag_m and $(AgCl)_n$ clusters can be well described. Also the two clusters Ag_{115} and $(AgCl)_{192}$ are large enough to mimic bulk properties in the core and surface states on the outside of the crystallite. From this we deduce that it is most reasonable to choose the Ag_{115}–$(AgCl)_{192}$ composite illustrated in Figure 4 as the main object for further investigations.

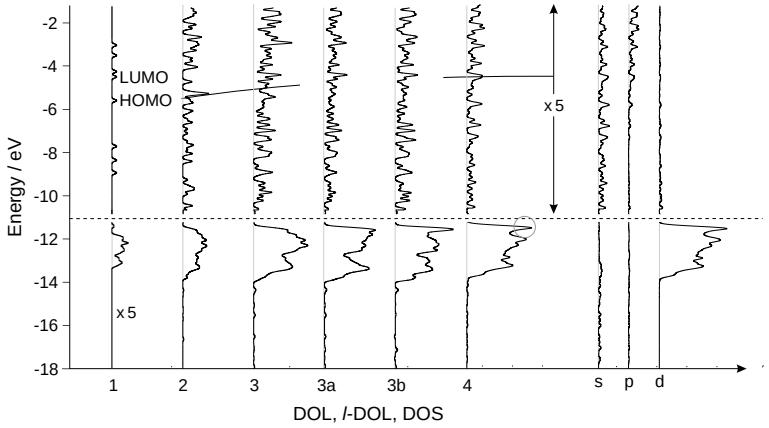

Figure 6. DOL, *l*-DOL of Ag_m clusters, and DOS of Ag_∞, Ag_9 (1), Ag_{115} (2), Ag_{276} (3), Ag_{276} without the outermost shell (3a), Ag_{276} without the two outermost shells (3b), and DOS of the periodic infinite crystal (4). The HOMO is marked with a line. The peak at the upper d-band level in the crystal overlaid by SURS in the clusters is marked with a gray circle. The s, p, and d band region of the infinite system is projected (s, p, d). DOL and DOS above the dashed line at -11 eV are scaled up five times, for they would be too small to show differences otherwise. The same applies for the whole Ag_9 DOL.

Positions of the Ag_{115} on top of the $(AgCl)_{192}$: The first question to be answered is that of the stability of a Ag_m cluster on top of a $(AgCl)_n$ cluster with respect to the separated parts. Several positions and cluster–cluster distances were investigated in order to answer this question. The most stable positions were found when the center of the Ag_{115} lies above the diagonal line of the $(AgCl)_{192}$ consisting of chloride ions. The progress of the optimization is shown in Figure 7, in which

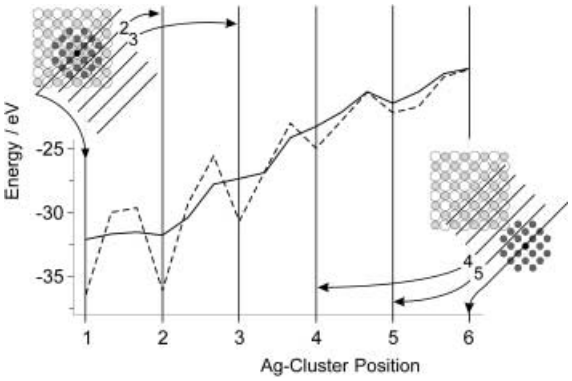

Figure 7. Stabilization energy of a Ag_{115} cluster, when shifted along the $(AgCl)_{192}$ surface, shown at optimized $Ag_{115}-(AgCl)_{192}$ distances. The vertical lines serve as orientation for the reader. The center of the Ag_{115} cluster is marked with a black circle. As that cluster is moved and crosses a marked line (numbers 1–6), the associated energy may be found by looking at the corresponding vertical line in the graph. The two extreme positions (1, 6) are shown in the inset detail. The energy for the position shown in the inset (——) and that after rotating the Ag_{115} cluster by 45° (- - - -) is also indicated (cf Figure 4).

each position corresponds to an optimized $Ag_{115}-(AgCl)_{192}$ distance. The geometry of an unstable (right) and the most stable position (left) is shown in the inset. As a further degree of freedom, rotation of the Ag cluster was allowed. We distinguish between the 0° position shown in Figure 7 (line) and a position where the Ag cluster is rotated by 45° (dashed), see Figure 4 for details. Positions in between were found to be less stable. Geometries in which the silver cluster center lies directly above a chloride ion, were always found to be the most stable. There is an oscillatory behavior, which is more pronounced in the 45° case that finally ends in the absolute minimum (Position 1 in Figure 7).

The shortest $Ag_{115}-(AgCl)_{192}$ composite distance for the 0° case was calculated to be 3.0 Å. The distance is measured perpendicular to the component clusters. The global minimum was found for the 45° case and a 2.8 Å intercluster separation. The slightly shorter bond length at 45° is due to a larger number of bonding interactions between the silver atoms of the Ag_m and the chlorine atoms of the $(AgCl)_n$, for geometrical reasons. This geometry was used for all further calculations, including the $Ag_{409}-(AgCl)_{192}$ composite discussed below.

Net charge distribution: What is the charge distribution in such a composite? We investigated slabs taken parallel to the interface. It turned out that it is easier to view the results for a larger silver cluster on top of the $(AgCl)_{192}$ cluster, namely the $Ag_{409}-(AgCl)_{192}$ composite, see Figure 3, bottom right. The summed up total charges for each of the 23 slabs are shown in Figure 8 (×), while in addition cuts I (○) and II (●)—as defined in Figure 4—are shown. The charges calculated for the same slabs but at infinite $Ag_{409}-\infty-(AgCl)_{192}$ separation are marked by a gray line.

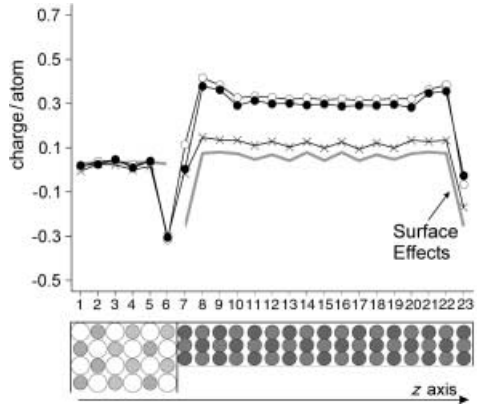

Figure 8. Total net charges of the individual slabs 1, 2, 3, …, 23 of the $Ag_{409}-(AgCl)_{192}$ composite. Crosses (×) mark the summed up total net charges of each slab. The cuts I (○) and II (●), described in Figure 4 have been projected. The net charges of the individual cluster $(AgCl)_{192}$ and Ag_{409} (same geometry but at infinite separation) are shown as a gray line. Changes of net charges due to surface states are indicated with an arrow.

We first note that the crosses and this gray line are parallel, with the exception of the interface slabs 6, 7, and 8. This indicates that the interface layer extends only over one AgCl (which picks up negative charge) and two Ag slabs (which donate charge to the AgCl interface slab). Cuts I and II reveal additional information. They show that the core of the silver cluster is positively charged with respect to the surface, and especially that the core of slab 8 donates a lot of electrons. The charges on slabs 23, 22, and 21 illustrate what happens at the metal–vacuum interface. The surface slab picks up charge first from the adjoining layer, the next deeper one, and also deeper lying atoms. This means that Ag_n clusters are, in general, negatively charged at the surface and positively charged in the core. This smoothes out with increasing cluster size.

A more detailed charge-distribution analysis of the $Ag_{115}-(AgCl)_{192}$ composite is given in Figure 9. We report the difference in charge between the infinitely separated clusters $Ag_{115}-\infty-(AgCl)_{192}$ and the composite, as a function of the energy. The HOMO of the isolated $(AgCl)_{192}$ and the work function of the isolated Ag_{115} clusters are marked with horizontal lines. Energy levels in which a slab acts as an electron donor or as an electron acceptor can be recognized. Values pointing to the right of the vertical lines refer to an uptake of electrons, values pointing to the left to a donation of electrons. In the energy range between -16 and -5 eV, a transfer of electrons from the Ag cluster slab 7 to the AgCl cluster layer 6 is observed. But the region between -10 to -6 eV is where we find the AgCl band gap. How can electrons be transferred to the AgCl bandgap region, where no states nominally are available? As we will see, this is due to states in the bandgap induced by Ag_m clusters adsorbed on AgCl clusters. Although the major electron transfer occurs at the

  0947-6539/02/0808-1790 $ 20.00+.50/0 *Chem. Eur. J.* **2002**, *8*, No. 8

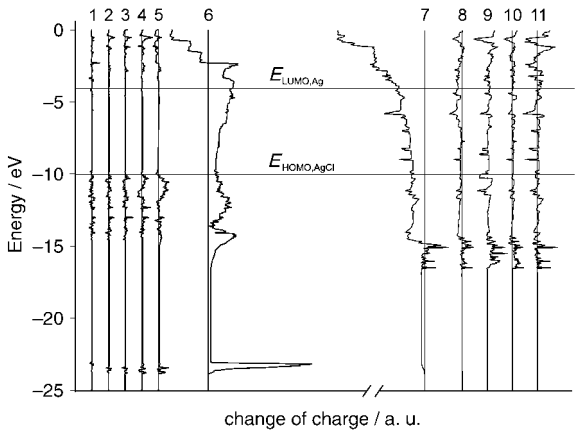

Figure 9. Change of charge of the $Ag_{115}-(AgCl)_{192}$ composite with respect to the individual clusters (separated system). The same numbering as in Figure 4 is used. The HOMO of the $(AgCl)_{192}$ and the LUMO of the Ag_{115} cluster are marked with a line, which serve for orientation. Cut II is used for this representation.

junction, up to three layers are involved. Layers 4 and 5 show changes in the d-orbital region of the AgCl from -12 to -10 eV, but almost no electron increase in the band gap region.

Metal induced gap states (MIGS) and metal induced d states (MIdS): The main reason for the charge transfer from the silver cluster to the silver chloride cluster is the newly formed MIGS[52] in slab 6 in the energy range between -10 and -6 eV, but also MIdS at about -15 eV. They are the result of an interaction of wave functions of the two clusters, mainly the orbitals of the two adjacent AgCl and Ag slabs 6 and 7. The MIGS are easy to observe because they are induced in an energy region where otherwise no levels exist. It is more difficult to analyze MIdS because they overlay some AgCl d states.

Figure 10 gives insight into the properties of the MIGS and MIdS. Figure 10a shows the *l*-DOL of slab 6 in the energy range between -18 and -3 eV of a $Ag_{115}-(AgCl)_{192}$ composite (——) and of a separated cluster system $Ag_{115}-\infty-(AgCl)_{192}$ (- - - -). The newly formed states of the composite below -15 eV, marked with a circle, are induced by the d states of the Ag_{115}. These d states contribute to the MidS, which lie on average 1 eV below the $4d-(AgCl)_{192}$ orbitals.

Above -10 eV, where the AgCl bandgap is expected, a number of newly formed states occur. These are the MIGS. Detailed analysis shows that Ag_{115} wave functions mix with orbitals of both the chloride and the silver ions of the $(AgCl)_{192}$. Nearest-neighbor interactions dominate with the important exception of the silver ion corner atoms of the $(AgCl)_{192}$.

The enlarged $l-$DOL in the energy range from -10 eV to -5 eV in Figure 10b gives more insight in the MIGS properties of slab 6. The first gap states are induced at -9 eV. At -7 eV, the MIGS are overlaid by states derived from the Ag corner atoms of the AgCl cluster (SURS). These atoms behave in a special way, and are the object of a closer view in Figure 10c. The *l*-DOL of slab 6 of Ag corner atoms in an isolated $(AgCl)_{192}$ shows a sharp peak at -7 eV that corresponds to SURS, as we discussed in more detail in ref. [10]. In contrast, the *l*-DOL of the same atom but now in the $Ag_m-(AgCl)_n$ composite is broadened and split in energy. This shows that the localization of the SURS is annihilated by the remarkable interaction with Ag_{115} states. A similar broadening of the Cl-3s orbitals of slab 6 at -25 eV occurs (not shown). However, only nearest neighbor interactions of the Cl^- ions with the adjacent silver cluster are responsible for this. The Cl^- corner ions are not influenced and show a sharp peak.

Figure 11 shows a comparison of the MIGS in the band gap region between -10 eV and -5 eV between slab 6 (——) and the spread contributions of slabs 5 (- - - -) and 4 (••••). The MIGS contribution of slab 5 is about ten times smaller with respect to slab 6 and the individual weights change. That contribution further decreases rapidly in slab 4 and nearly vanishes in the energy range between -10 eV and -7.5 eV. MIGS in slabs further away from the interface appear to become negligibly small.

Conclusion

Silver clusters show strong bonding interaction with a silver chloride surface; we calculate that the $Ag_{115}-(AgCl)_{192}$ and similar composites shown in Figure 3 are stable with respect to the separated cluster system $Ag_{115}-\infty-(AgCl)_{192}$. We have developed a set of tools for analyzing the vast amount of numbers produced by the computer. The role of ionic defects in silver halides has been reviewed in detail by Maier.[53] It has not been considered in the present study, in which we focus on the electronic properties of the clusters and composites in Figure 3, from which some general conclusions can be derived. The charge distribution analyzed slab by slab and also as

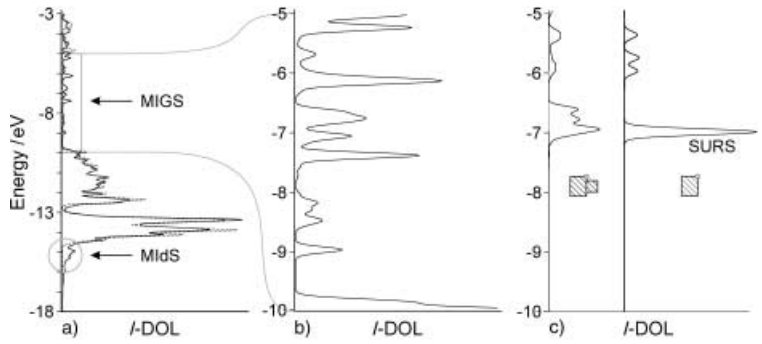

Figure 10. a) *l*-DOL of slab 6 in the energy range between -18 and -3 eV of the $Ag_{115}-(AgCl)_{192}$ composite (——) and the separated cluster system $Ag_{115}-\infty-(AgCl)_{192}$ (- - - -). b) Enlarged *l*-DOL of slab 6 in the band gap region between -10 and -5 eV. c) Enlarged *l*-DOL of two representative silver corner atoms. Left: Corner atom of layer 6 of the composite. Right: Corner atom of layer 6 of a separated cluster system $Ag_{115}-\infty-(AgCl)_{192}$.

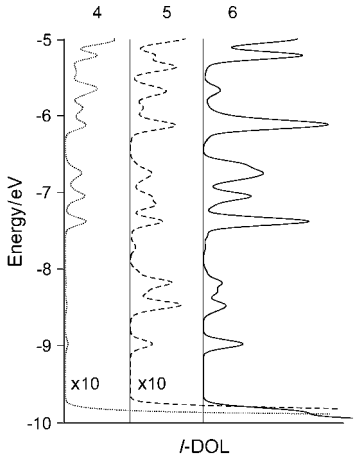

Figure 11. *l*-DOL of slab 6 (——), slab 5 (- - - -), and slab 4 (••••) in the band gap region between − 10 and − 5 eV. Slabs 4 and 5 are magnified by a factor of 10.

function of the energy revealed remarkable details of the microscopic features at the interface; these result in a net electron donation from the Ag_m to the $(AgCl)_n$ cluster. Analysis of the DOL and the *l*-DOL in the $(AgCl)_n$ bandgap region of the $Ag_{115}-(AgCl)_{192}$ composite allowed us to identify the MIGS and MIdS, the origin of which is the interaction between the wave functions of the two clusters. These novel and important states are quite localized in nature; nearest neighbor interactions dominate in them, with the important exception of the $(AgCl)_{192}$-SURS. Especially the MIGS should be detectable in specific spectroscopic experiments. Their penetration depth is limited to the first AgCl slab with small and very small contributions in the second and the third one, respectively. A comparison of the DOL of an $(AgCl)_{192}$ cluster and the *l*-DOL of the $(AgCl)_{192}$ part of the composite with the phenomenological picture of silver clusters on a silver chloride surface taken from ref. [5] is illustrated in Figure 12. It shows that the valence band position is only little influenced by the formation of MIGS.

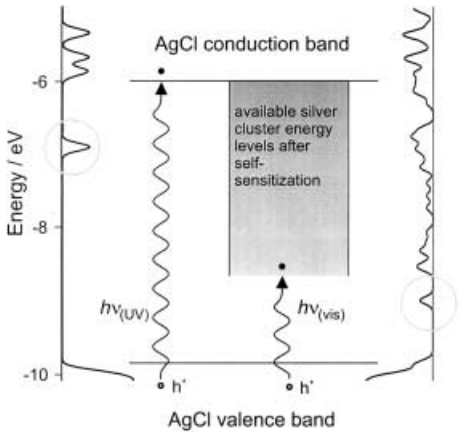

Figure 12. Proposed mechanism of self-sensitization. DOL of a $(AgCl)_{192}$ cluster is shown on the left and the *l*-DOL of the $Ag_{115}-(AgCl)_{192}$ composite is shown on the right. We observe new induced levels below the LUMO of the AgCl cluster. A schematic view is shown in the middle. The lowest lying levels into which electrons can be excited are marked with a gray circle (left: SURS, right: MIGS). The position of the valence band is not markedly influenced by the Ag_{115}.

The occupation of the MIGS and the silver cluster levels is governed by thermal distribution and can be tuned by Ag^+ ion absorption at the surface. This causes empty states accessible by electronic absorption processes, a phenomenon which affects greatly the photosensitivity of such systems.

Acknowledgements

We acknowledge financial support from the Schweizerisches Bundesamt für Energiewirtschaft BEW, project no. 76645, and from the Schweizerische Nationalfonds zur Förderung der wissenschaftlichen Forschung, project NF 2000/061259.00. The work at Cornell was supported by the US National Science Foundation through Research Grant CHE-99-70089. We thank Professor Gary Hodes for helpful discussions and suggestions.

Appendix

Charge iteration procedure for $d^{10}s^1$ and $d^{10}s^2$ elements: We have reconsidered the charge iteration parameters for silver according to the procedure described in refs. [20, 24, and 54] and by using the spectroscopic data for the Ag atom reported by Moore.[55] The values are listed in Table 2 and implemented in ICON-EdiT.[20] The procedure has been described in detail in the literature.[54, 56] The procedure used so far causes problems for d^{10}, $d^{10}s^1$, and $d^{10}s^2$ configurations. We explain a procedure which solves this problem.

The Coulomb integral H_{ii} used in EHMO calculations is equal to the negative value of the valence state ionization energy (VSIE) of the atomic orbital *i*. The VSIE is evaluated in terms of both an atomic charge Q and a configuration appropriate for that atom when incorporated in the molecule of interest. Thus:

$$H_{ii} = E(Q+1) - E(Q) = -\sum_c a_c \,\mathrm{VSIE}\,(\mathrm{configuration}_c, Q) \qquad (1)$$

here the electron that is removed and that increases the excess charge to $Q + 1$ is taken from the atomic orbital *i*. The charge dependence of the VSIE can be expressed with good accuracy as:

$$\mathrm{VSIE}\,(\mathrm{configuration}, Q) = d_0 + d_1 Q + d_2 Q^2 \qquad (2)$$

The coefficients d_0, d_1, and d_2 are determined from spectroscopic data. Three electronic configurations are usually considered for an appropriate description of the H_{ii} Coulomb integrals of transition elements. For example:

$$\begin{aligned} -H_{pp}(d^\delta s^\sigma p^\pi) = {} & (2-\sigma-\pi)\mathrm{pVSIE}(d^{n-1}p^1) \\ & + (\pi-1)\mathrm{pVSIE}(d^{n-2}p^2) + \sigma\mathrm{pVSIE}(d^{n-2}s^1p^1) \end{aligned} \qquad (3)$$

This equation shows that interpolation of $H_{pp}(d^\delta s^\sigma p^\pi)$ for different electron configurations $d^\delta p^\pi s^\sigma$ is certainly valid within the following limits:

$$s^\sigma (0 \le \sigma \le 1)$$

$$p^\pi (1 \le \pi \le 2)$$

$$d^\delta (n-2 \le \delta \le n-1) \qquad (4)$$

Values obtained too far outside of these limits must be considered more carefully. The problem can best be demonstrated by splitting Equation (3) in two parts, one for the σ occupation and one for the π occupation:

$$\begin{aligned} s(\sigma) &= -\sigma\mathrm{pVSIE}(d^{n-1}p^1) + \sigma\mathrm{pVSIE}(d^{n-2}s^1p^1) \\ &= \sigma[\mathrm{pVSIE}(d^{n-2}s^1p^1) - \mathrm{pVSIE}(d^{n-1}p^1)] \end{aligned} \qquad (5)$$

$$\begin{aligned} p(\pi) &= (2-\pi)\mathrm{pVSIE}(d^{n-1}p^1) + (\pi-1)\mathrm{pVSIE}(d^{n-2}p^2) \\ &= 2\mathrm{pVSIE}(d^{n-1}p^1) - \mathrm{pVSIE}(d^{n-2}p^2) + \pi[\mathrm{pVSIE}(d^{n-2}p^2) - \mathrm{pVSIE}(d^{n-1}p^1)] \end{aligned} \qquad (6)$$

  0947-6539/02/0808-1792 $ 20.00+.50/0 *Chem. Eur. J.* **2002**, *8*, No. 8

The Coulomb integral can be expressed as:

$$-H_{pp}(d^{\delta}s^{\sigma}p^{\pi}) = p(\pi) + s(\sigma) \tag{7}$$

Inserting the values for silver we obtain:

$$s(\sigma) = \sigma(4.67\ \text{eV} - 3.83\ \text{eV}) = \sigma 0.84\ \text{eV} \tag{8}$$

$$\begin{aligned} p(\pi) &= 2 \times 3.83\ \text{eV} - 8.12\ \text{eV} + \pi[8.12\ \text{eV} - 3.83\ \text{eV}] \\ &= -0.46\ \text{eV} + \pi 4.29\ \text{eV} \end{aligned} \tag{9}$$

$$-H_{pp}(d^{\delta}s^{\sigma}p^{\pi}) = -0.46\ \text{eV} + \pi 4.29\ \text{eV} + \sigma 0.84\ \text{eV} \tag{10}$$

From this follows that small π-values can lead to a change of sign of $H_{pp}(d^{\delta}s^{\sigma}p^{\pi})$. This is physically not acceptable. In addition, it can not only seriously affect the numerical stability of the charge iteration procedure but also lead to completely wrong Coulomb integrals. This becomes especially problematic when dealing with large systems. We have seen that the problem arises from the fact that, for example, the electron configuration $d^{9.7}p^{0.05}s^{0.25}$ is not correctly treated. We need an additional data point to handle the region $p^{\pi} = (0 \leq \pi \ll 1)$ correctly. This data point can be obtained by asking: What is the value of $pVSIE(d^{10}p^{0}s^{1})$? Since the p orbital is empty, $pVSIE(d^{10}p^{0}s^{1})$ is equal to zero:

$$pVSIE(d^{10}p^{0}s^{1}) = 0 \tag{11}$$

With this value, the problem can be solved by using a quadratic interpolation. We write:

$$s(\sigma) = a_s + b_s\sigma \tag{12}$$

$$s(\pi) = a_p + b_p\pi a_s + c_p\pi^2 \tag{13}$$

$$-H_{pp}(d^{\delta}s^{\sigma}p^{\pi}) = p(\pi) + s(\sigma) \tag{14}$$

From Equation (5), and substituting for $s(\sigma)$:

$$\begin{aligned} a_s &= 0 \\ b_s &= pVSIE(d^{n-2}s^{1}p^{1}) - pVSIE(d^{n-1}p^{1}) \end{aligned} \tag{15}$$

This means that $s(\sigma)$ poses no problems. The values of a_p, b_p, and c_p can be calculated by considering the following three situations:

$$p(\pi = 0) = pVSIE(d^{n-1}s^{1}p^{0}) = 0 \tag{16a}$$

$$p(\pi = 1) = pVSIE(d^{n-1}p^{1}) \tag{16b}$$

$$p(\pi = 2) = pVSIE(d^{n-2}p^{2}) \tag{16c}$$

From this follows:

$$p(1)\colon\ 0 + b_p 1 + c_p 1^2 = pVSIE(d^{n-1}p^{1}) \tag{17a}$$

$$p(2)\colon\ 0 + b_p 2 + c_p 2^2 = pVSIE(d^{n-2}p^{2}) \tag{17b}$$

Which leads to:

$$\begin{aligned} b_p &= \tfrac{1}{2}pVSIE(d^{n-2}p^{2}) + 2pVSIE(d^{n-1}p^{1}) \\ c_p &= \tfrac{1}{2}pVSIE(d^{n-2}p^{2}) + pVSIE(d^{n-1}p^{1}) \end{aligned} \tag{18}$$

We can combine Equations (13) and (18):

$$p(\pi) = \left[\frac{\pi - 1}{2}pVSIE(d^{n-2}p^{2}) + (2 - \pi)pVSIE(d^{n-1}p^{1})\right]\pi \tag{19}$$

Both, $s(\sigma)$ and $p(\pi)$ are zero for $\sigma = 0$ and $\pi = 0$, respectively, which is correct. In addition, $-H_{pp}(d^{\delta}s^{\sigma}p^{\pi})$ will never change sign for any physically acceptable pVSIE values.

[1] W. Schottky, *Naturwissenschaften* **1938**, *26*, 843.
[2] J. O. Nylander, F. Masszi, S. Selberherr, S. Berg, *Solid State Electron.* **1989**, *32*(5), 363.
[3] E. H. Rhoderick, R. H. Williams, *Metal–Semiconductor Contacts*, Clarendon, Oxford, **1988**.
[4] P. Würfel, *Physik der Solarzellen*, Spektrum, Heidelberg/Berlin, **1995**.
[5] M. Lanz, D. Schürch, G. Calzaferri, *J. Photochem. Photobiol. A* **1999**, *120*, 105.
[6] M. Alducin, S. P. Appell, *Nucl. Instrum. Methods Phys. Res. Sect. B* **2000**, *164–165*, 662.
[7] J. Jamnik, J. Maier, S. Pejovnik, *Solid State Ionics* **1995**, *80*, 19.
[8] A. P. Marchetti, A. A. Muenter, R. C. Baetzold, R. T. McCleary, *J. Phys. Chem. B* **1998**, *102*, 5287.
[9] J. Maier, U. Lauer, W. Göpel, *Solid State Ionics* **1990**, *40/41*, 463.
[10] S. Glaus, G. Calzaferri, *J. Phys. Chem. B* **1999**, *103*, 5622.
[11] R. Seifert, R. Rytz, G. Calzaferri, *J. Phys. Chem. B* **2000**, *104*, 7473.
[12] M. Brändle, G. Calzaferri, M. Lanz, *Chem. Phys.* **1995**, *201*, 141.
[13] J. D. Head, K. A. R. Mitchell, L. Noodleman, *Surf. Sci.* **1977**, *69*, 714.
[14] A. Rochefort, D. R. Salahub, A. Phaedon, *J. Phys. Chem. B* **1999**, 103, 641.
[15] I. Tamm, *Z. Physik* **1932**, *76*, 849.
[16] R. Hoffmann, *J. Chem. Phys.* **1963**, *39*, 1397.
[17] R. Hoffmann, *Solids and Surfaces: A Chemist's View of Bonding in Extended Structures*; VCH, New York, **1988**.
[18] G. Calzaferri, L. Forss, I. Kamber, *J. Phys. Chem.* **1989**, *93*, 5366.
[19] G. Calzaferri, R. Hoffmann, *J. Chem. Soc. Dalton Trans.* **1991**, 917.
[20] G. Calzaferri, R. Rytz, M. Brändle, D. Brühwiler, S. Glaus, *ICON-EDiT, Extended Hückel Molecular Orbital and Transition Dipole Moment Calculations*; available at http://iacrs1.unibe.ch, update **2000**.
[21] G. Calzaferri, R. Rytz, M. Brändle, D. Brühwiler, S. Glaus, *BICON-CEDiT, Extended Hückel Tight-Binding and Crystal Transition Dipole Moment Calculations*; available at http://iacrs1.unibe.ch, update **2000**.
[22] D. Brühwiler, N. Gfeller, G. Calzaferri, *J. Phys. Chem. B* **1998**, *102*, 2923.
[23] A. H. MacDonald, *Phys. Rev. B: Condens. Matter* **1978**, *18*, 5897.
[24] H. Basch, A. Viste, H. B. Gray, *Theor. Chim. Acta* **1965**, *3*, 458.
[25] R. S. Mulliken, *J. Chem. Phys.* **1955**, *23*, 1833.
[26] S. Karthäuser in *Proc. IS&T/SPSTJ's International Symposium on Silver Halide Imaging*: *"Silver Halide in a New Millennium"*, Sainte-Adèle, Québec, Canada, IS&T, Springfield, VA, **2000**, 25.
[27] U. Kreibig, M. Vollmer, *Optical Properties of Metal Clusters*, Springer, **1995**, p. 25.
[28] P. L. Freund, M. Spiro, *J. Phys Chem.* **1985**, *89*, 1074.
[29] A. Henglein, B. G. Ershov, M. Malow, *J. Phys. Chem.* **1995**, *99*, 14129.
[30] S. Fafard, *Photonics Spectra* **1997**, *31*, 160.
[31] T. H. James, *The Theory of the Photographic Process*, 4th ed. Macmilan, New York, **1977**.
[32] K. Kneipp, L. T. Perelman, H. Kneipp, V. Backman, A. Jorio, G. Dresselhaus, M. S. Dresselhaus, *Phys. Rev. B: Condens. Matter* **2001**, *63*(19), 193411.
[33] D. V. Averin, K. K. Likharev, *Mesosc. Phenom. Solids* **1991**, 169.
[34] M. Westphalen, U. Kreibig, J. Rostalki, H. Lüth, D. Meissner, *Sol. Energy Mater. Sol. Cells* **2000**, *61*, 97.
[35] G. Calzaferri, D. Brühwiler, S. Glaus, D. Schürch, A. Currao, C. Leiggener, *J. Imaging Sci. Technol.* **2001**, *45*, 331.
[36] C. Jackschath, I. Rabin, W. Schulze, *Z. Phys D* **1992**, *22*, 517.
[37] G. Alameddin, D. Hunter, D. Cameron, M. M. Kappes, *Chem. Phys. Lett.* **1992**, *192*, 122.
[38] M. Chelvayohan, C. H. B. Mee, *J. Phys. C: Solid State Phys.* **1982**, *15*, 2305.
[39] V. Bonačić-Kouteký, L. Češpiva, P. Fantucci, J. Koutecký, *Z. Phys. D* **1993**, *26*, 287.
[40] J. Zhao, X. Chen, G. Wang, *Phys. Stat. Sol B* **1995**, *188*, 719.
[41] E. Schumacher, *Chimia* **1988**, *42*, 357.
[42] M. Seidl, M. E. Spina, M. Brack, *Z. Phys D* **1991**, *19*, 101.
[43] M. D. Wood, *Phys. Rev. Lett.* **1981**, *46*(11), 749.
[44] E. E. Krasovskii, A. N. Yaresko, V. N. Antonov, *J. Elect. Spect. Relat. Phenom.* **1994**, *68*, 157.
[45] S. Fedrigo, W. Harbich, J. Buttet, *Phys. Rev. B* **1993**, *47*(16), 10706.
[46] H. Neddermeyer, *J. Phys. F* **1982**, L241.
[47] A. Goldmann, E. Bartels, *Surf. Sci.* **1982**, *122*, L629.
[48] S. D. Kevan, N. G. Stoffel, N. V. Smith, *Phys. Rev. B* **1985**, *32*, 4956.

[49] H. Erschbaumer, A. J. Freeman, C. L. Fu, R. Podloucky, *Surf. Sci.* **1991**, *243*, 317.
[50] P. H. Miller, J. W. M. DuMond, *Phys. Rev.* **1940**, *57*(2), 198.
[51] For bond distance optimization the following Coulomb parameters have been used: $H_{ss} = -7.84$ eV, $H_{pp} = -1.11$ eV, $H_{dd} = -15.42$ eV.
[52] W. Mönch, *Phys Rev. B: Condens. Matter* **1988**, *37*, 7129.
[53] J. Maier, *Prog. Solid State Chem.* **1995**, *23*(3), 171.
[54] S. P. McGlynn, L. G. Vanquickenborne, M. Kinoshita, D. G. Carroll, *Introduction to Applied Quantum Chemistry*, Hoft, Rinehart and Winston, New York, **1972**.
[55] C. E. Moore, *Atomic Energy Levels Vol. 3*, National Bureau of Standards, Washington, **1971**.
[56] C. J. Ballhausen, H. B. Gray, *Molecular Orbital Theory*, Benjamin, New York, **1965**.

Received: September 24, 2001 [F3569]

  0947-6539/02/0808-1794 $ 20.00+.50/0